Surface & Coatings Technology 385 (2020) 125326

Contents lists available at ScienceDirect

Surface & Coatings Technology

journal homepage: www.elsevier.com/locate/surfcoat

Effect of WC content on microstructures and mechanical properties of FeCoCrNi high-entropy alloy/WC composite coatings by plasma cladding

Yingbo Peng[b], Wei Zhang[a,*], Tianchen Li[a], Mingyang Zhang[a], Bin Liu[a], Yong Liu[a], Li Wang[c], Songhao Hu[d]

[a] Powder Metallurgy Research Institute, Central South University, Changsha 410083, China
[b] College of Engineering, Nanjing Agricultural University, Nanjing 210031, China
[c] Department Metal Physics, Helmholtz-Zentrum Geesthacht, Geesthacht 21502, Germany
[d] Henan Huanghe Whirlwind Co., Ltd., Xuchang 461500, China

ARTICLE INFO

Keywords:
Metal matrix composite coating
FeCoCrNi
WC
Plasma cladding
Microstructure
Mechanical properties

ABSTRACT

FeCoCrNi high-entropy alloy/WC composite coatings were fabricated via plasma cladding on steels adding different mass fraction of WC. Effects of WC content on the microstructure and mechanical properties of the coatings were studied. The results showed that WC content significantly affected microstructure and the wear resistance of the coatings. With the increase of WC content, the microstructures of the coatings became complex. When WC content was more than 60%, the coatings consisted of WC, FCC phase of HEA matrix as metal bond, Fe_3W_3C carbide phase and Cr-rich secondary solid solution phase. The Fe_3W_3C carbides improved the hardness and wear resistance of the coating. When WC content was at a high proportion of 60%, the HEA/WC coating had the best wear resistance with the minimum volume wear rate of 3.27×10^{-7} $mm^3/N{\cdot}m$ and the high hardness of 59.6 HRC, which was better than commercial Ni60/WC coating with the same WC content.

1. Introduction

Metal matrix composite (MMC) coatings have good comprehensive properties and have been widely used as wear-resistant coatings in many fields [1–3]. A lot of efforts have been made to improve the wear resistance of MMC coatings, including adding or forming in-situ ceramic strengthening phases in the coating, such as TiB_2, TiC, TiB, Al_2O_3, and WC [4–6]. However, many problems are often encountered in practical applications, such as uneven distribution of reinforcement particles, micro-defects, low bonding strength between reinforcement particles and metal matrix in MMC coatings [7,8]. These problems are attributed to the poor retention and wettability of the metal matrix, especially with high proportion of strengthening phase, which would limit the further increasing of the volume fraction of strengthening phases. Moreover, the serious interfacial reaction between the metal matrix and the reinforcement particles would deteriorate the performance of the coating.

Unlike traditional alloys, which are doped with complex alloying elements to improve properties, high-entropy alloys (HEAs), as a new multi-principal alloy system, have unique microstructure and properties [9,10]. Moreover, its excellent retention and wettability to reinforcement particles can make up for the defects of traditional metal matrix and solve the above problems to a large extent [11,12]. It is suitable for usage as metal matrix material for wear-resistant MMC and its coatings and provides the possibility of adding high proportion strengthening phase. Some efforts have been put into the HEA/WC composite and relevant coatings, these researches show some advantages in microstructure and mechanical properties [13–15].

There are many techniques to produce MMC coatings, such as plasma spraying, magnetron sputtering, laser cladding, surface welding, and plasma cladding [16–20]. Among many methods of MMC coating preparation, plasma cladding technology has the advantages of simple maintenance, low cost and wide material adaptability [21,22]. Because its heating and cooling rate is lower than that of laser cladding, the melting pool can be maintained for a long time, which will be conducive to the formation of homogenized structures, and the defects will be greatly reduced. Therefore, plasma cladding technology has significant advantages in the preparation of MMC coatings with high hardness and wear-resistance.

In this study, the composite coatings with FeCoCrNi HEA matrix as metal bond and WC particles as reinforcements were successfully prepared by plasma cladding. The effects of WC addition on microstructures, interfacial behavior of WC/HEA interface and wear properties of the coatings were investigated. In addition, under the same

* Corresponding author.
E-mail address: waycsu@csu.edu.cn (W. Zhang).

https://doi.org/10.1016/j.surfcoat.2019.125326
Received 3 November 2019; Received in revised form 27 December 2019; Accepted 28 December 2019
Available online 10 January 2020
0257-8972/

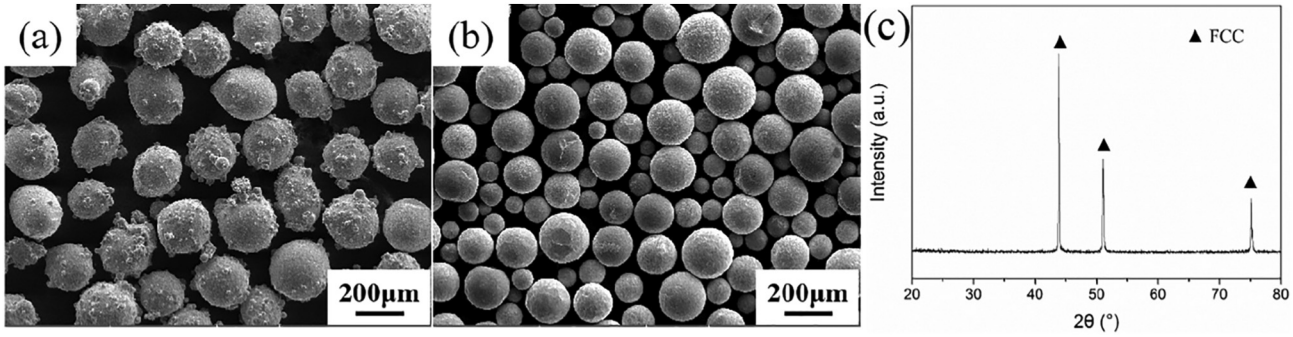

Fig. 1. SEM morphology of (a) FeCoCrNi pre-alloyed powders and (b) spherical WC particles, (c) XRD pattern of FeCoCrNi pre-alloyed powders.

wear conditions, the wear properties of HEA/WC coating were compared with that of commercial Ni60/WC wear-resistant coating.

2. Experimental

The investigated HEA coatings with different mass fraction (10%, 20%, 40%, 60%, 70%) of spherical WC reinforcing particles were prepared by plasma cladding. The nominal composition of HEA was $Fe_{25}Co_{25}Cr_{25}Ni_{25}$ (in at. %) which was a face-centered cubic (FCC) structure [23], and the substrate was a 42CrMo (ASTM 4140). The HEA powder was prepared by gas atomization method (atomization temperature: 1600 °C, medium: argon, pressure: 3–4 atm, nozzle size: 4 cm). The morphology of FeCoCrNi HEA powder is shown in Fig. 1(a). It can be seen that HEA powder is spherical and uniform in size. In the process of atomization, due to the difference of cooling rate, small melts cooled faster, and thus adhered to the surface of large droplets to form satellite structure. Fig. 1(c) is the XRD pattern of HEA powder. The 2θ of 43.84°, 51.07° and 75.14° corresponding to the diffraction peaks are (111), (200), (220) respectively, which fit the diffraction peaks of the FCC phase. This illustrates that the FeCoCrNi HEA powder prepared by atomization is composed of single-phase FCC solid solution. Fig. 1(b) shows that the spherical WC powder has complete sphericity and smooth surface without obvious defects. There is no obvious agglomeration in the HEA and WC powders.

The parameters of plasma cladding used are shown in Table 1. A FEI Quanta FEG 250 scanning electron microscope (SEM) equipped with an energy-dispersive X-ray (EDX) analyser was used to investigate the microstructure and chemical compositions of the MMC coating (20 kV, using spot analysis and backscattering mode). A philips CM 200 transmission electron microscopy (TEM) operated at 200 kV was used to identify the structures by selected area electron diffraction (SAED) analysis. The TEM specimen was prepared by a crossbeam workstation AURIGA 40 (Zeiss, Germany) equipped with a focused ion beam (FIB) column and scanning electron microscopy (SEM). For more accurate compositional analyses, an electron probe microanalyses (EPMA, JXA-8530F, Japan) was used. The Rockwell hardness of C Gauge was measured by using Wilson RB2000 hardness tester and was averaged from three measurements. The microhardness was measured by using a nanoindenter (UNHTL + MCT, Switzerland) with a load of 10 mN for 10 s. The wear tests were conducted on a high-speed reciprocating friction testing machine (HSR-2 M, Lanzhou) under the load of 50 N and a sliding speed of 9 m/min at room temperature. The counterpart was Si3N4 ball (φ = 6 mm). Every sample was tested 3 times, and the results were averaged.

Table 1
Plasma cladding parameters preparing FeCoCrNi/WC MMC coatings.

Parameters	Plasma Cladding
Current (A)	40
Ionized gas flow rate (L/min)	2.5
Powder feeding gas rate (L/min)	3.0
Spray distance (mm)	80
Traverse speed (mm/s)	2.0

3. Results and discussions

3.1. Phase identification and microstructures

Fig. 2 is the XRD diffraction pattern of HEA/WC MMC coatings with different content of spherical WC particles prepared by plasma cladding. The mass fractions of WC were 0%, 10%, 20%, 40%, 60% and 70%, respectively. It can be seen that the coating consists of a single FCC phase without adding WC, which was consistent with the phase structure of the original HEA powder. When the WC content increased to 10%, there was no diffraction peak of new phase. However, when the WC content increased to 20%, the diffraction peaks of Fe_3W_3C (M_6C) appeared, and the intensity of this peak increased with the increase of WC content, which indicates that the proportion of the Fe_3W_3C carbide increases. In addition, when the WC content is 20%, the diffraction peaks of W_3C appear, which indicated that the decomposition and decarbonization of WC were serious in the cladding process. When the WC content continued to rise, the W_3C peaks disappeared and the diffraction peaks of WC and W_2C phases appeared, which indicated that the decomposition of WC was inhibited and WC particles were well preserved.

Fig. 3 shows the cross-sectional microstructures of FeCoCrNi/WC MMC coatings with different spherical WC contents. It can be seen from Fig. 3(a) that the FeCoCrNi HEA coating exhibited a single contrast in the backscattering electron mode of SEM. FeCoCrNi high entropy alloy is considered as one of the most stable HEA alloys [23]. It is difficult to

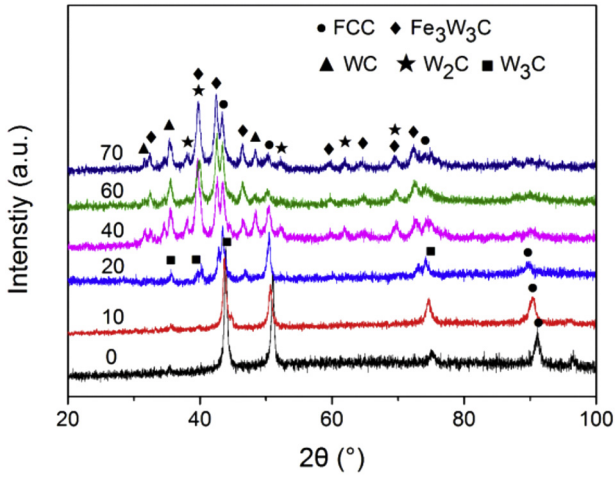

Fig. 2. X-ray diffraction (XRD) pattern of FeCoCrNi/WC MMC coatings with different WC content.

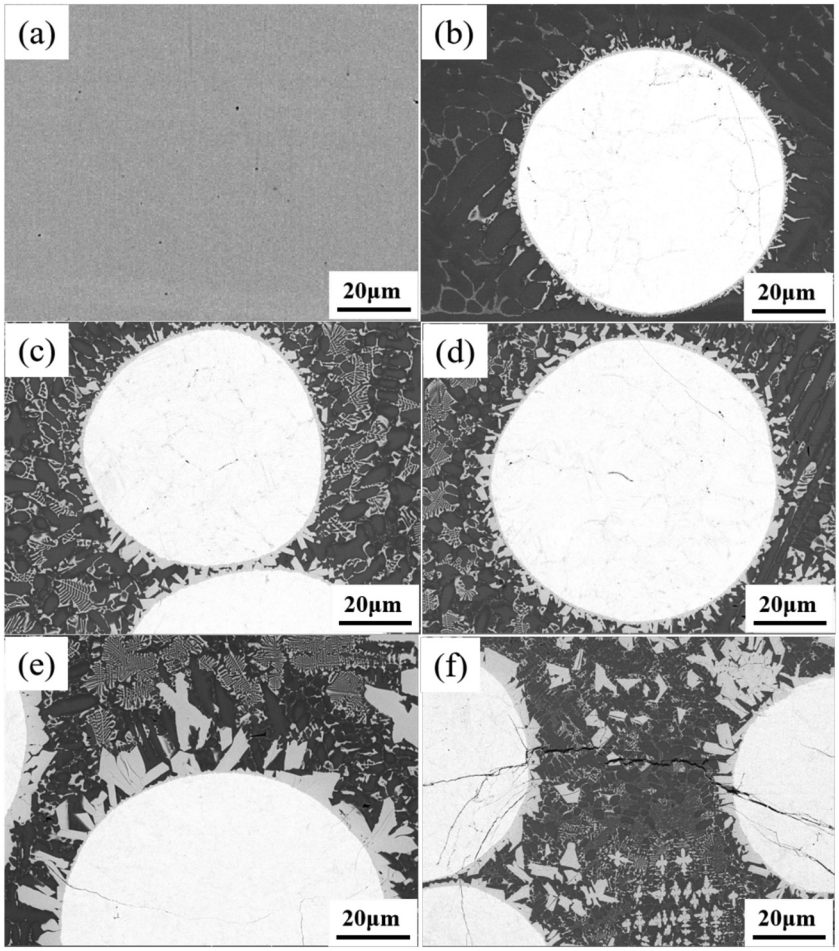

Fig. 3. Microstructures of FeCoCrNi/WC MMC coatings with different amount of WC: (a) 0%, (b) 10%, (c) 20%, (d) 40%, (e) 60%, (f) 70%.

realize the phase transformation from this stable FCC structure without adding the alloying elements like Al, Mo and Nb, etc. [24–26], indicating that the FeCoCrNi HEA coating prepared by plasma cladding had a single FCC structure with no second phase precipitation. When WC content was 10%, WC and HEA matrix diffused each other. WC particles gradually decomposed and formed a narrow transition layer, a small amount of fine filamentary structure formed on the edge of WC particles structure were precipitated around the transition layer, as shown in Fig. 3(b). With the increase of WC content to 20% and 40%, massive structure precipitated around the transition layer, massive carbides formed on the edge of WC particles, and fishbone structure formed among the WC particles, as shown in Fig. 3(c) and (d). When the WC content was 60% and 70%, the massive structures at the transition layer grew significantly, the content of fishbone structures in HEA matrix increased, and the dendritic structures began to appear in the coatings, as shown in Fig. 3(d) and (f). Moreover, when the WC content was 70%, cracks appeared in the cladding layer. In Fig. 3(f), cracks can be observed between adjacent WC particles. The appearance of cracks mainly caused by the increase of volume fraction of carbides with the increasing of WC particle addition, and the FCC phase as binder agent decreased significantly. Thermal expansion coefficients of WC particles and HEA were different, under the condition of rapid heating and cooling in plasma cladding, the thermal stress produced by cladding exceeded the strength limit of the HEA matrix, which results in cracks.

There were three morphologies of precipitations in the coatings and the composition of the precipitations are analyzed by EPMA, as shown in Fig. 4 and Table 2. The HEA matrix, massive, fishbone and dendritic structures correspond to point A, B, D and E in Fig. 5, respectively. It can be seen that the composition of massive, fishbone and dendritic structures were similar. Compared with HEA matrix, Fe content decreased greatly while Cr content increased in these structures, so it is inferred that Fe element was replaced by Cr, and the replaced Fe and W formed the M_6C carbides of Fe_3W_3C. According to EPMA analysis and XRD results, it can be determined that the carbides of three different morphologies in the coating were Fe_3W_3C phase (M_6C). M_6C carbides have the characteristics of strong eutectic growth of microcrystalline plane, usually exhibit a eutectic growth of dendrite clusters on radial radiation microcrystalline plane. Therefore, fishbone and dendritic carbides were formed in the coating. The coating structures were mainly divided into three parts: the main body of WC particles, the fusion zone between the surface layer of WC particles and HEA (primary massive carbides) and the diffusion zone of HEA matrix (fishbone and dendritic eutectic carbides). The morphology evolution of this carbide was related to the amount of WC addition. The type of carbides produced during cladding basically did not change, and the content of eutectic carbides in the coating increased gradually.

In order to observe the bonding area between WC particles and HEA matrix, elemental mapping of composite coatings containing 70% WC was carried out by EPMA, as shown in Fig. 5. Because dendritic carbides were located far from WC particles in HEA matrix, massive carbides adhering to WC particles and fishbone eutectic carbides in HEA matrix were observed. The Fe, Cr and Ni elements in the coatings were more distributed in HEA matrix than in carbides. Comparing massive carbides with fishbone carbides, it was found that the Fe, Co, and Ni content of massive carbides was lower than that of fishbone carbides, while the W content was higher. This is because massive carbides are the primary carbides produced by directly diffusion from WC particles, while fishbone carbides are carbides formed by decomposition of WC

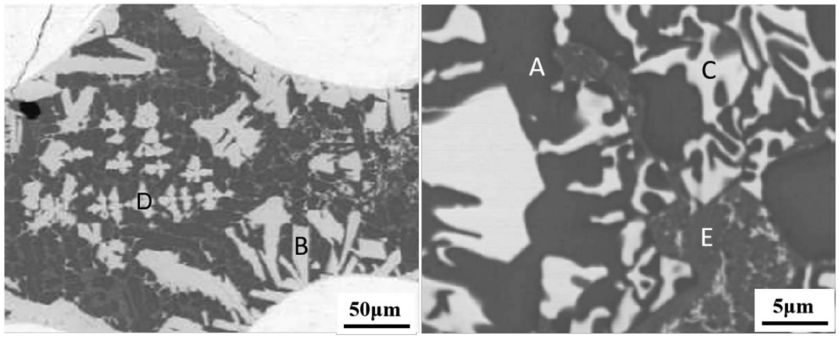

Fig. 4. Microstructures in FeCoCrNi/WC MMC coatings with 70% WC addition.

Table 2
Chemical compositions by EPMA of different microstructure in Fig. 5.

At. %	Fe	Co	Cr	Ni	W	C
A (HEA matrix)	40.32	16.78	18.63	17.44	2.99	3.84
B (massive)	27.79	8.92	7.26	7.01	38.53	10.49
C (fishbone)	35.74	7.20	9.81	5.65	31.76	9.84
D (dendrite)	31.33	7.64	9.63	5.42	35.30	10.68
E (network)	25.56	19.40	26.25	8.33	3.38	15.05

particles and eutectic reaction of free C atoms into HEA matrix.

The W and C exhibited gradient distribution, which of W and C decreased from the WC particles to the surrounding HEA matrix. However, there were some obvious segregations in C in Fig. 5, which coincided with the enrichment region of Fe, Co and Cr, but poor in W. The composition of the network structures are shown as point E in Fig. 4 and Table 2. These network-shape precipitates were not found on XRD pattern in Fig. 2. Due to the high mixing entropy effect of HEAs promotes the mutual solubility of each principal component, and form simple solid solution structure [27]. According to the model of regular solution [28], when n types of element with equal molar ratio form a solid solution, the formula for calculating the mixing entropy is:

$$\Delta S = \mathrm{R}\ln(n) \quad (1)$$

where R is the ideal gas constant (8.314 J/kmol).

According to the formula, the entropy change ΔS is very large when a multi-principal alloy forms a solid solution. Therefore, when C to diffuse into HEA, the free C atoms preferentially dissolve into HEA matrix and form secondary solid solution without forming the carbides or intermetallics. So, the network structures were the solid solution phase, which were poor in W but rich in Fe, Co, Cr and C. When the solid solubility of C in secondary Cr-rich solid solution reached saturation, and free C in HEA matrix would form carbides as Fe_3W_3C.

The microstructures of the MMC coating were further identified by TEM. The sampling location is shown in Fig. 6 (a), including the massive carbides around the interface, the fishbone carbides and the HEA matrix. Fig. 6 (b) shows the TEM bright field image of Fe_3W_3C carbide and HEA. It can be seen that the carbides initially exhibited massive shape, and gradually changed to fishbone shape as the carbides continued to grow into HEA. Obviously, both forms of Fe_3W_3C carbides were continuous and the same kind. The HEA matrix and Fe_3W_3C carbides all exhibited face centred cubic structure which corresponded to the results of XRD and EPMA, as shown in Fig. 6(c) and (d).

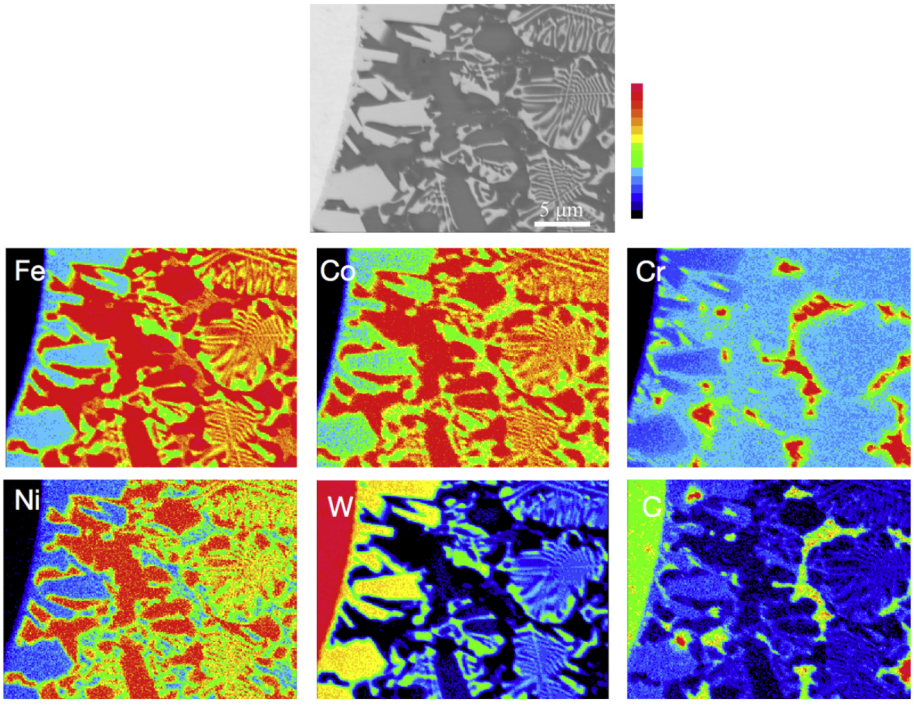

Fig. 5. Elemental mapping at the HEA/WC interface in MMC coatings with 70% WC addition.

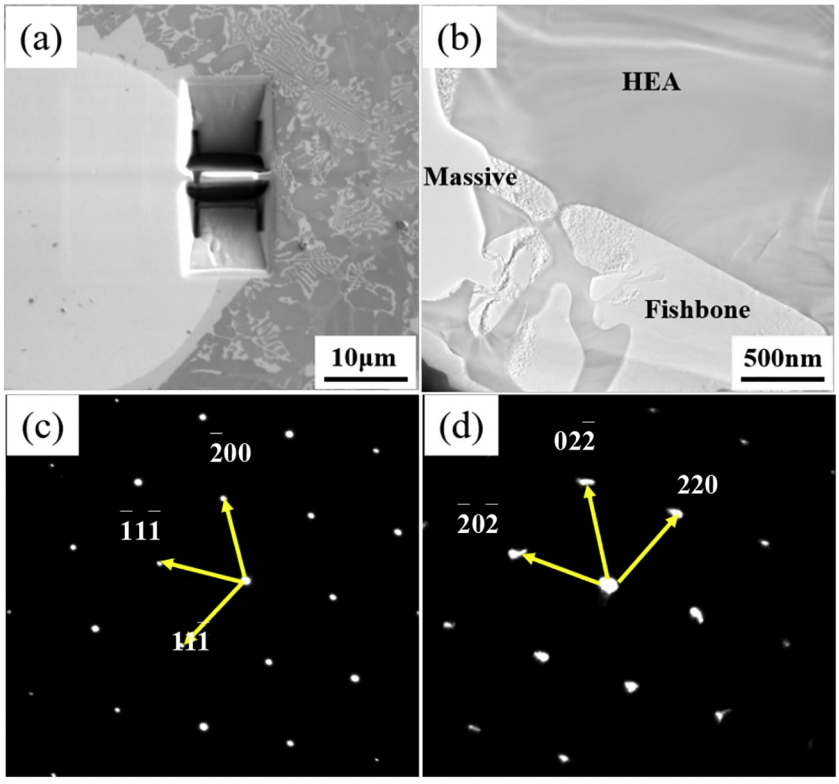

Fig. 6. TEM image of FeCoCrNi/WC MMC coatings with 70% WC addition: (a) Sampling location by FIB, (b) bright field image, (c) SAED of HEA matrix, (d) SAED of Fe_3W_3C.

3.2. Hardness

The hardness of the FeCoCrNi/WC MMC coatings was tested, as shown in Table 3. It can be found that the higher WC particle content, the hardness of the coatings increased. When the WC content was 10%, the hardness of MMC coating was only 29.5 HRC. With the increase of WC content to 40%, the growth trend of hardness slowed down. Finally, when the WC content was 70%, the hardness reached 61.9 HRC. There are two reasons for the increase of hardness of coatings. On the one hand, WC is a common strengthening phase with high hardness, which is close to diamond. Therefore, the higher the WC content, the higher the hardness of the coating. On the other hand, with the increase of WC content, the higher the concentration of free W and C in HEA matrix after dissolution and diffusion of WC particles, more carbide phases will precipitate, which are generally hard and brittle, thus increasing the hardness of the coatings. The dissolution of WC particles increases the hardness of coatings, which is the result of various strengthening mechanisms. The dissolution of WC particles makes alloying elements W and C dissolved into solid solution, which plays a role of solid solution strengthening; various forms of carbides produce second phase strengthening; precipitated carbides play a role in fine grain strengthening of equiaxed HEA matrix.

In order to reflect the effect of different microstructures on hardness, nanoindentation tests were carried out on MMC coatings with 70% WC content, as shown in Fig. 7. The hardness of WC particles, massive Fe_3W_3C, fishbone and dendritic Fe_3W_3C, secondary Cr-rich solid solution and HEA matrix were 3335.9 HV, 2225.4 HV and 2323.4 HV, 883.1 HV and 465.3 HV, respectively. The hardness of fishbone and dendritic Fe_3W_3C carbides was basically the same, which was consistent with the similar composition of the two morphologies in Table 2. The primary massive carbides were formed without complete diffusion with the HEA matrix, the alloying degree of Fe as well as hardness were slightly lower than fishbone and dendritic carbides. The hardness of the matrix was 465 HV, which was much higher than that of the FeCoCrNi coating (260 HV) without WC. The HEA matrix occurs interstitial solution strengthening due to the entry of C element of the dissolved WC particles. Solid solution of interstitial atoms in HEAs, such as C, O, P, B and N, can play a good role of strengthening in HEA [29–32]. Because of the small size of interstitial atoms, the lattice distortion of HEAs can be larger, so the strengthening effect of HEAs is significantly greater than that of substitutional solid solution strengthening. The hardness of secondary Cr-rich solid solution phase is doubled than that of HEA matrix due to the introduction of large amounts of Co, Cr and C. It is also a strengthening phase in the composite coatings.

3.3. Wear properties

The friction coefficient curves of FeCoCrNi/WC coating is shown in Fig. 8 (a). When WC content was 10%, the friction coefficient was unstable and fluctuated greatly in the process of friction due to the uneven distribution of WC particles. The friction coefficient increased with time, and finally reached 0.8. With the increase of WC content, the friction coefficient curve tended to be stable. When WC content was 20%, 40%, 60% and 70%, the friction coefficient of the coating was 0.69, 0.45, 0.42 and 0.35 respectively. With the increase of WC content,

Table 3
The hardness of FeCoCrNi/WC MMC coatings with different WC content.

WC content	0	10	20	40	60	70
HRC	24.0 ± 0.5	29.5 ± 1.2	41.7 ± 3.6	53.2 ± 2.0	59.6 ± 2.8	61.9 ± 1.7

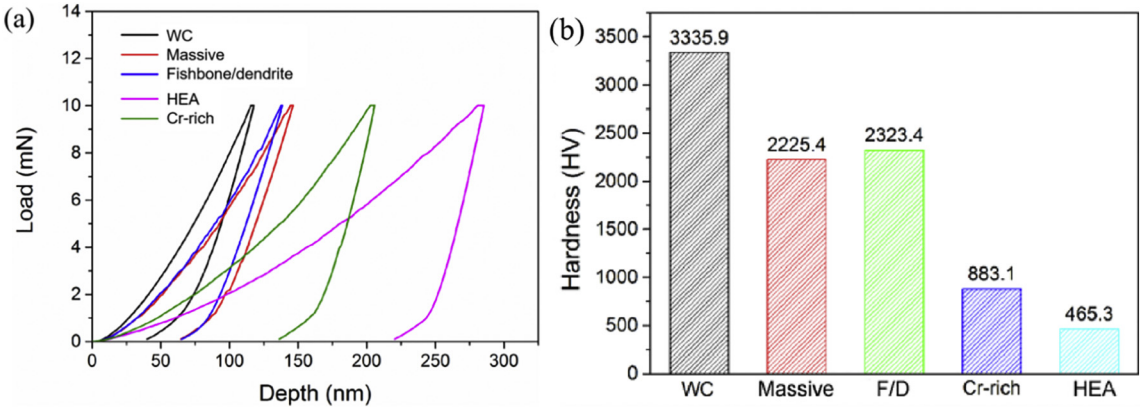

Fig. 7. (a) Load-depth and (b) hardness curves of different phases in FeCoCrNi/70%WC coatings.

the friction coefficient of the coating decreased gradually, indicating that the lubrication effect of the coating was gradually enhanced. When WC particles were added, WC would exist in the cladding layer in the form of hard phase. WC particles have high hardness, good wear resistance, strong deformation resistance in the process of friction, and are not easy to plastic deformation, resulting in large friction resistance, which limits the growth of friction coefficient. In addition, the friction properties of HEA/WC MMC coating were compared with that of commercial Ni-based alloy/WC MMC coating with 60 wt% WC particles added (abbreviated as Ni60/WC) [7,33,34]. The friction coefficient of Ni60/WC was 0.35, which was similar to that of HEA/70WC coating.

Fig. 8(b) shows the relationship between volume wear rate of HEA/WC MMC coating with different WC content. With the increase of WC content, the wear resistance of the coating firstly increased and then decreased. When WC content was 10%, the volume wear rate of the coating was as high as 3.03×10^{-5} mm^3/N·m. With the increase of WC content, the volume wear rate of the coating decreased gradually. When WC content is 60%, the wear rate reached the minimum value of 3.27×10^{-7} mm^3/N·m, but it rised to 8.57×10^{-7} mm^3/N·m when WC content was 70%.

It is known that the higher the hardness is, the better the wear resistance is. However, the coating with HEA/70WC had high hardness but poor wear resistance. This abnormally may be caused by cracks on the surface of WC particles and HEA matrix in HEA/70WC coating, resulting in WC particles easily broken and peeled off during the friction process. In contrast, the volume wear rate of Ni60/WC coating was 8.83×10^{-7} mm^3/N·m, which is 2.5 times of HEA/60WC coating. Therefore, the HEA/WC coating prepared by plasma cladding in this study had excellent wear resistance when WC content was 60%, which was also significantly improved compared with the commercial Ni60/WC wear-resistant coating.

The worn surface morphology of HEA/WC MMC coatings are shown in Fig. 9. It can be seen from Fig. 9. (a) that when the WC content was 10%, obvious delamination appeared on the worn surface of the coating, accompanied by a large number of grooves, indicating that this sample was a wear mechanism combining adhesive wear and abrasive wear. The breakage of WC particle was serious and the retention on WC particles was poor, which indicated that the wear resistance of the HEA/10WC coating was poor. The formation of delaminations on the worn surface was attributed to the residual stress in the coatings after the cladding. In the process of friction, the stress concentration was easy to occur under the friction and shear stress, and then microcracks were generated. These microcracks formed the crack source. In the subsequent friction process, the crack expanded and then peeled off and delaminations occurred. When the content of WC was 40%, as shown in Fig. 9(b), the delamination in HEA/10WC disappeared. Although there were still a lot of grooves on the worn surface, the WC particles remained intact, which shows that the wear process was dominated by abrasive wear. When the content of WC increased to 60%, as shown in Fig. 9(c), the worn surface became smooth and no grooves are found. WC particles were well retained and only a small area of local fracture occurred. The HEA/60WC coating can effectively withstand and resist the plastic deformation under repeated cutting and extrusion of Si3N4 ball during friction. The worn surface of HEA/60WC coating was observed in the backscatter electron mode of SEM, as shown in Fig. 9 (d). It can be clearly observed that the massive, fishbone and dendrite carbide phases in the coating were well preserved, and there were no obvious grooves during the friction process. Because there were many

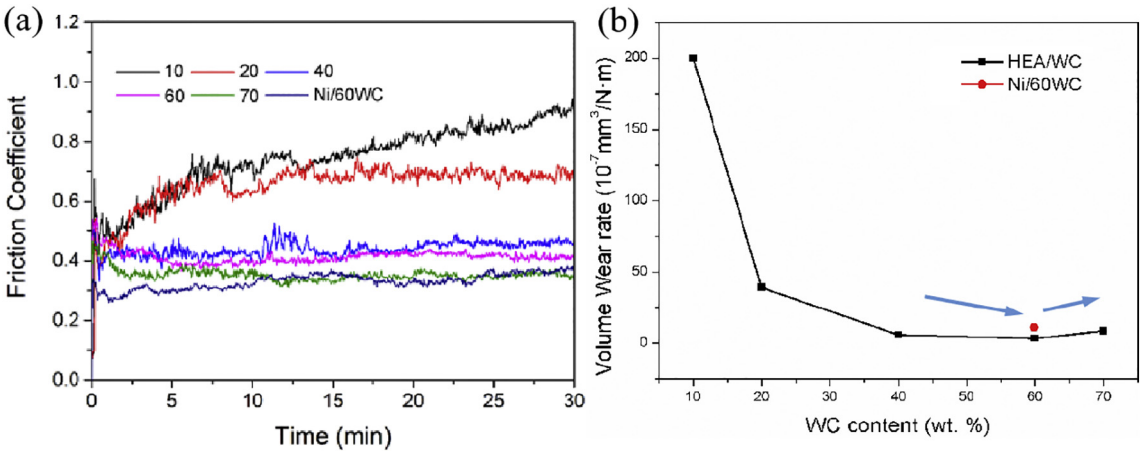

Fig. 8. (a) The friction coefficients and (b) volume wear rates of the FeCoCrNi/WC MMC coatings and Ni60/WC coating.

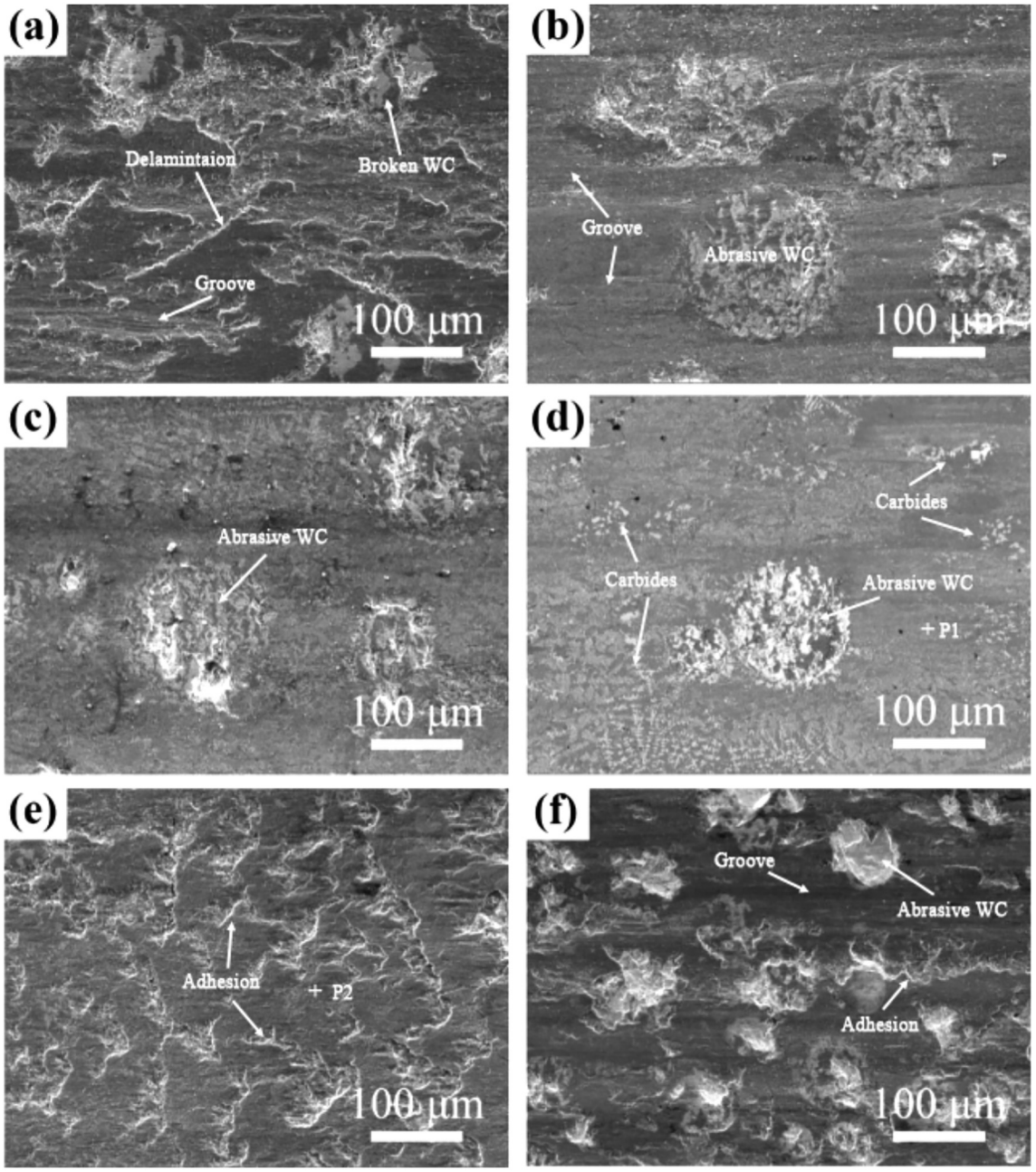

Fig. 9. Worn surface morphologies of the coatings: FeCoCrNi/WC MMC coatings with WC content of (a) 20%, (b) 40%, (c) 60%, (d) 60% in BSE image, (e) 70% and (f) Ni60/WC coating.

Fe_3W_3C carbide hard particles dispersed in the coating, which can resist the cutting effect of debris during friction. So the grooves were shallow and difficult to observe and reduced the wear rate of the coating. The results show that the high hardness Fe_3W_3C phase have a good friction reducing effect, and improve the wear resistance of the MMC coating.

When the content of WC increased to 70%, the wear resistance of the coating began to decline. In Fig. 9 (e), it was found that the WC particles in the worn surface were not intact and there were a lot delamination on the surface, which indicated that the WC particles in the coating fall off during the friction and adhesive wear occurred on the HEA matrix. Although the WC content and hardness of HEA/70WC coating were the highest, due to the reduction of the volume fraction of the plastic HEA matrix, the retention of HEA matrix on WC particles was reduced, which lead to a large number of WC particles falling off during the friction process. In addition, due to the high cooling rate in plasma cladding process and the different thermal expansion coefficient between HEA and WC, microcracks appeared in the coating under the action of thermal stress. Under the action of external load, the stress concentration occurred at the crack, and the crack accelerated to expand, so that the wear rate of the coating increased significantly. The EDS analysis of P1 and P2 marked in Fig. 9 (d) and (e) shown in Table 4 shows that the oxygen content in the worn surface of HEA/70WC coating increased sharply compared with HEA/60WC coating, indicating that the coating was oxidized during the wear process, and the

Table 4
EDS analysis of P1 and P2 in worn surfaces marked in Fig. 9(d) and (e).

	Fe	Co	Cr	Ni	W	C	O	Si
P1	30.55	16.97	17.67	14.80	4.25	7.83	5.53	2.4
P2	22.28	8.77	9.00	8.68	1.73	8.36	36.98	4.19

oxidation products were mainly metal oxides. Due to the peeling off of WC particles, the HEA matrix in the coating was in direct contact with Si_3N_4 ball. As a lot of heat was generated during the friction process, the metallic elements of HEA reacted with oxygen to form oxide films, which were easily peeled off during the friction process. Thus, continuous delaminations appeared on the worn surface.

It can be seen from Fig. 9 (f) that, as the comparison sample, although the WC particles in the Ni60/WC coating were relatively small and well dispersed, the retention of the bonding HEA phase was weakened during the wear process due to the lower hardness and weaker bonding force of the Ni-based alloy matrix than that of the HEA matrix. The broken and falling WC particles acted as abrasive particles on the worn surface and the alloys matrix directly participated in friction. With the reciprocating motion of the Si3N4 ball, grooves and delaminations were formed, showing an abrasive wear mechanism accompanied by adhesion wear. The wear resistance was lower than HEA/60WC coating.

4. Conclusions

(1) FeCoCrNi HEA coatings with WC reinforced particles of 10–70 wt% addition were successfully prepared by plasma cladding.
(2) With the increase of WC content, the microstructures of the MMC coatings became more complex. When WC content was more than 60%, Fe_3W_3C carbide with different morphologies and Cr-rich secondary solid solution phase precipitated in the coatings.
(3) The evolution of Fe_3W_3C carbides of the coatings with the increase of WC content was: initial massive carbide at WC/HEA interface → eutectic fishbone carbides → dendrite carbide in HEA matrix.
(4) As the volume fraction of carbides increased, the hardness of the coating increased. When the WC content was 70%, the hardness reached 61.9 HRC.
(5) The HEA matrix had a good retention on WC particles and the Fe_3W_3C carbide phase had a good friction reducing effect. With a high WC proportion of 60%, the MMC coating had the best wear resistance (better than Ni60/WC coating with same WC content), and the minimum volume wear rate was 3.27×10^{-7} mm^3/N·m.

Author contributions

Conceptualization, W.Z. and B.L.; Methodology, W.Z. and S.H.H.; Validation, Y.B.P.; Formal Analysis, W.Z. and Y.B.P.; Investigation, M.Y.Z. and T.C.L.; Resources, Y.L., L.W. and S.H.H.; Data Curation, T.C.L. and S.H.H.; Writing-Original Draft Preparation, T.C.L. and M.Y.Z.; Writing-Review & Editing, W.Z. and Y.B.P.; Project Administration, W.Z. and Y.L.; Funding Acquisition, Y.L. and S.H.H.

Declaration of competing interest

The authors declare that they have no known competing financial interests or personal relationships that could have appeared to influence the work reported in this paper.

Acknowledgements

The authors wish to acknowledge the financial support of State Key Laboratory of Powder Metallurgy (CSU 621011808), the National Natural Science Foundation of China (51731006), the introduction projects of high-end foreign experts in 2019 for strategic science and technology development, Ministry of Science and Technology of the China (No: G20190010113), the Starting Research Fund of Nanjing Agricultural University (RCQD-1803).

References

[1] M.K. Akbari, H.R. Baharvandi, K. Shirvanimoghaddam, Tensile and fracture behavior of nano/micro TiB_2, particle reinforced casting A356 aluminum alloy composites, Mater. Des. 66 ((2015) 150–161.
[2] Y.H. Diao, K.M. Zhang, Microstructure and corrosion resistance of TC_2 Ti alloy by laser cladding with Ti/TiC/TiB_2 powders, Appl. Surf. Sci. 352 (2015) 163–168.
[3] H. Tan, Z. Luo, Y. Li, F. Yan, R. Duan, Y. Huang, Effect of strengthening particles on the dry sliding wear behavior of Al_2O_3-M_7C_3/Fe metal matrix composite coatings produced by laser cladding, Wear 324 (2015) 36–44.
[4] S.F. Zhou, X.Q. Dai, Laser induction hybrid rapid cladding of WC particles reinforced NiCrBSi composite coating, Appl. Surf. Sci. 256 (2010) 4708–4714.
[5] T. Yu, Q.L. Deng, J.F. Zheng, G. Dong, J.G. Yang, Microstructure and wear behaviour of laser clad NiCrBSi+Ta composite coating, Surf. Eng. 28 (2013) 357–363.
[6] L. He, Y.F. Tan, X.L. Wang, Q.F. Jing, X. Hong, Tribological properties of laser cladding TiB_2 particles reinforced Ni-base alloy composite coatings on aluminum alloy, Rare Metals 34 (2015) 1–8.
[7] Q.S. Ma, Y.J. Li, J. Wang, K. Liu, Microstructure evolution and growth control of ceramic particles in wide-band laser clad Ni60/WC composite coatings, Mater. Des. 92 (2016) 897–905.
[8] X.H. Wang, M. Zhang, B.S. Du, S. Li, Microstructure and wear properties of laser clad (TiB_2+TiC)/Fe composite coating, Surf. Rev. Lett. 19 (2012) (295-234).
[9] M.H. Chuang, M.H. Tsai, W.R. Wang, S.J. Lin, J.W. Yeh, Microstructure and wear behavior of Alx$Co_{1.5}$Cr$FeNi_{1.5}$Tiy high-entropy alloys, Acta Mater. 59 (2011) 6308–6317.
[10] N.D. Stepanov, N.Y. Yurchenko, V.S. Sokolovsky, M.A. Tikhonovsky, G.A. Salishchev, An AlNbTiV$Zr_{0.5}$ high-entropy alloy combining high specific strength and good ductility, Mater. Lett. 161 (2015) 136–139.
[11] W. Zhang, M.Y. Zhang, Y.B. Peng, L. Wang, Y. Liu, S.H. Hu, Y. Hu, Interfacial behavior of multiple structures and mechanical properties of a high-entropy alloy/diamond composite, Int. J. Refract. Met. H. 86 (2020) 105109.
[12] W. Zhang, M.Y. Zhang, Y.B. Peng, F.Z. Liu, Y. Liu, S.H. Hu, Y. Hu, Effect of Ti/Ni coating of diamond particles on microstructure and properties of high-entropy alloy/diamond composites, Entropy 21 (2019) 164.
[13] Y.B. Peng, W. Zhang, T.C. Li, M.Y. Zhang, L. Wang, Y. Song, S.H. Hu, Y. Hu, Microstructures and mechanical properties of FeCoCrNi high entropy alloy/WC reinforcing particles composite coatings prepared by laser cladding and plasma cladding, Int. J. Refract. Met. H. 84 (2019) 105044.
[14] W.Y. Luo, Y.Z. Liu, Y. Luo, M. Wu, Fabrication and characterization of WC-AlCoCrCuFeNi high-entropy alloy composites by spark plasma sintering, J. Alloy Compd. 754 (2018) 163–170.
[15] R. Zhou, G. Chen, B. Liu, J.W. Wang, L.L. Han, Y. Liu, Microstructures and wear behaviour of (FeCoCrNi)1-x(WC)x high entropy alloy composites, Int. J. Refract. Met. H. 75 (2018) 56–62.
[16] J.Y. Xu, B.L. Zou, S.Y. Tao, M.X. Zhang, X.Q. Cao, Fabrication and properties of Al_2O_3-TiB_2-TiC/Al metal matrix composite coatings by atmospheric plasma spraying of SHS powders, J. Alloy Compd. 672 (2016) 251–259.
[17] M.J. DAI, C.B. Wei, K.S. Zhou, M. Zhu, H.J. Hou, S.S. Lin, X. Tong, Properties of W/DLC/W-S-C composite films fabricated by magnetron sputtering, Trans. Nonferrous Met. Soc. China 25 (2015) 3002–3011.
[18] K. Liu, Y.J. Li, J. Wang, In-situ reactive fabrication and effect of phosphorus on microstructure evolution of Ni/Ni-Al intermetallic composite coating by laser cladding, Materi. Des. 105 (2016) 171–178.
[19] Y.F. Liu, J.S. Mu, X.Y. Xu, S.Z. Yang, Microstructure and dry-sliding wear properties of TiC-reinforced composite coating prepared by plasma-transferred arc weld-surfacing process, Mater. Sci. Eng. A 458 (2007) 366–370.
[20] H.T. Cao, X.P. Dong, Z. Pan, X.W. Wu, Q.W. Huang, Y.T. Pei, Surface alloying of high-vanadium high-speed steel on ductile iron using plasma transferred arc alloying technique: microstructure and wear properties, Mater. Des. 100 (2016) 223–234.
[21] G.Z. Xie, X.L. Song, D.J. Zhang, Y.P. Wu, P.H. Lin, Microstructure and corrosion properties of thick WC composite coating formed by plasma cladding, Appl. Surf. Sci. 256 (2010) 6354–6358.
[22] C. Zhao, F. Tian, H.R. Peng, J.Y. Hou, Non-transferred arc plasma cladding of stellite Ni60 alloy on steel, Surf. Coat. Tech. 155 (2002) 80–84.
[23] B. Gludovatz, A. Hohenwarter, D. Catoor, E.H. Chang, E.P. George, R.O. Ritchie, A fracture-resistant high-entropy alloy for cryogenic applications, Science 345 (2014) 1153–1158.
[24] Y. Zhang, T.T. Zuo, Z. Tang, Microstructures and properties of high-entropy alloys, Prog. Mater. Sci. 61 (2014) 1–93.
[25] S.G. Ma, Y. Zhang, Effect of Nb addition on the microstructure and properties of AlCoCrFeNi high-entropy alloy, Mater. Sci. Eng. A 532 (2012) 480–486.
[26] W.H. Liu, J.Y. He, H.L. Huang, Effects of Nb additions on the microstructure and mechanical property of CoCrFeNi high-entropy alloys, Intermetallics 60 (2015) 1–8.
[27] J.W. Yeh, S.K. Chen, S.J. Lin, Nano-structured high entropy alloys with multiple principal elements: novel alloy design concepts and outcomes, Adv. Eng. Mater. 6 (2004) 299–303.
[28] K.C. Chou, S.K. Wei, A new generation solution model for predicting thermodynamic properties of a multicomponent system from binaries, Metall. Mater. Trans. B Process Metall. Mater. Process. Sci. 28 (1997) 439–445.
[29] Z.W. Wang, I. Baker, Z.H. Cai, S. Chen, J.D. Poplawsky, W. Guo, The effect of interstitial carbon on the mechanical properties and dislocation substructure evolution in $Fe_{40.4}Ni_{11.3}Mn_{34.8}Al_{7.5}Cr_6$ high entropy alloys, Acta Mater. 120 (2016) 228–239.
[30] N.D. Stepanov, D.G. Shaysultanov, R.S. Chernichenko, N.Y. Yurchenko, S.V. Zherebtsov, M.A. Tikhonovsky, G.A. Salishchev, Effect of thermomechanical processing on microstructure and mechanical properties of the carbon-containing CoCrFeNiMn high entropy alloy, J. Alloys Compd. 693 (2017) 394–405.
[31] Y.C. Xie, H. Cheng, Q.H. Tang, Effects of N addition on microstructure and

mechanical properties of CoCrFeNiMn high entropy alloy produced by mechanical alloying and vacuum hot pressing sintering, Intermetallics 93 (2018) 228–232.
[32] Y.W. Chen, Y.K. Li, X.W. Cheng, Interstitial strengthening of refractory $ZrTiHfNb_{0.5}Ta_{0.5}O_x$ (x = 0.05, 0.1, 0.2) high-entropy alloys, Mater. Lett. 228 (2018) 145–148.
[33] Q.H. Ma, Y.J. Li, J. Wang, K. Liu, Investigation on cored-eutectic structure in Ni60/WC composite coatings fabricated by wide-band laser cladding, J. Alloys Compd. 645 (2015) 151–157.
[34] D. Shu, Z.G. Li, K. Zhang, C.W. Yao, D.Y. Li, Z.B. Dai, In situ synthesized high volume fraction WC reinforced Ni-based coating by laser cladding, Mater. Lett. 195 (2017) 178–181.